1521-0111/90/1/42–51$25.00
MOLECULAR PHARMACOLOGY

http://dx.doi.org/10.1124/mol.116.103721
Mol Pharmacol 90:42–51, July 2016

N-Heterocyclic Carbene Capture by Cytochrome P450 3A4 [S]

Gareth K. Jennings, Caroline M. Ritchie, Lisa S. Shock, Charles E. Lyons, and John C. Hackett

Department of Physiology and Biophysics and the Massey Cancer Center, Virginia Commonwealth University School of Medicine, Richmond, Virginia

Received February 26, 2016; accepted April 27, 2016

ABSTRACT

Cytochrome P450 3A4 (CYP3A4) is the dominant P450 enzyme involved in human drug metabolism, and its inhibition may result in adverse interactions or, conversely, favorably reduce the systemic elimination rates of poorly bioavailable drugs. Herein we describe a spectroscopic investigation of the interaction of CYP3A4 with *N*-methylritonavir, an analog of ritonavir, widely used as a pharmacoenhancer. In contrast to ritonavir, the binding affinity of *N*-methylritonavir for CYP3A4 is pH-dependent. At pH <7.4, the spectra are definitively type I, whereas at pH ≥7.4 the spectra have split Soret bands, including a red-shifted component characteristic of a P450-carbene complex. Variable-pH UV-visible spectroscopy binding studies with molecular fragments narrows the source of this pH dependence to its *N*-methylthiazolium fragment. The C2 proton of this group is acidic, and variable-pH resonance Raman spectroscopy tentatively assigns it a pK_a of 7.4. Hence, this fragment of *N*-methylritonavir is expected to be readily deprotonated under physiologic conditions to yield a thiazol-2-ylidene, which is an *N*-heterocyclic carbene that has high-affinity for and is presumed to be subsequently captured by the heme iron. This mechanism is supported by time-dependent density functional theory with an active site model that accurately reproduces distinguishing features of the experimental UV-visible spectra of *N*-methylritonavir bound to CYP3A4. Finally, density functional theory calculations support that this novel interaction is as strong as the tightest-binding azaheterocycles found in P450 inhibitors and could offer new avenues for inhibitor development.

Introduction

The cytochrome P450 (P450) enzymes are involved in the biosyntheses of hormones and the disposition of xenobiotics (Guengerich, 2001; Denisov et al., 2005; Ortiz de Montellano, 2005). Inhibition of the dominant P450 in human drug metabolism, namely, cytochrome P450 3A4 (CYP3A4), has the potential to result in adverse drug-drug interactions by reducing the systemic elimination rates of coadministered drugs (von Moltke et al., 1998; Hollenberg, 2002; Lin et al., 2002; Rendic, 2002). Conversely, pharmacoenhancers exploit this effect and target CYP3A4 for therapeutic benefit by overcoming the rapid clearance, high dosing frequency, and subtherapeutic plasma concentrations characteristic of CYP3A4 substrates. The most successful application of this strategy has been applied in the treatment of human immunodeficiency virus and hepatitis C virus infections whereby ritonavir (Fig. 1) inhibits the clearance of antiviral therapeutics through inhibition of CYP3A4 (Kempf et al., 1995, 1997; Koudriakova et al., 1998; Hirsch et al., 2008; Klibanov et al., 2015).

Ritonavir is a high-affinity, type II P450 ligand that binds to CYP3A4 through hydrophobic interactions dominated by phenyl side chains and coordination of the thiazole nitrogen to the heme iron (Sevrioukova and Poulos, 2010). Structural modifications abolishing the phenyl groups substantially lower the affinity of these molecules for CYP3A4 and result in the observation of multiple ligand-binding orientations in their crystal structures (Sevrioukova and Poulos, 2013; Kaur et al., 2015). Nonetheless, thiazole coordination to the heme iron and orientation of the isopropyl thiazole unit near the protein surface remain consistent features of these structures. Moreover, CYP3A4 is capable of hydroxylating the isopropyl thiazole substituent, so the inverted binding mode orienting this end of the molecule toward the heme is indeed possible, though it has not been observed (Koudriakova et al., 1998). Owing to the observed hydroxylation, it has been suggested that the nitrogen atom in the isopropyl thiazole fragment does not appreciably coordinate to the heme (Sevrioukova and Poulos, 2010).

Akin to ritonavir, the majority of heme-coordinating P450 inhibitors are azaheterocycles where nitrogen atoms directly coordinate to iron; however, there are a few fragments where the coordinating atom is carbon. In these examples, the ligands are generally accepted to be carbenes generated by reductive or oxidative catalysis. For example, the red-shifted Soret band (450–470 nm) resulting from catalytic reduction of

This work was supported by the National Institutes of Health National Institute of General Medical Sciences [Grants R01GM092827, R01GM114168] and the Office of Naval Research [Grant N000141210773].
dx.doi.org/10.1124/mol.116.103721.
[S] This article has supplemental material available at molpharm.aspetjournals.org.

ABBREVIATIONS: CHAPS, 3-[3-(cholamidopropyl)dimethylammonio]-1-propanesulfonate; CYP3A4, cytochrome P450 3A4; DMSO, dimethylsulfoxide; HS, high spin; MDP, methylenedioxyphenyl-2-ylidene; MITV, N-[2-Isopropylthiazol-4-ylmethyl(methyl)carbamoyl]-L-valine; NMeR, *N*-methylritonavir; NMTI, *N*-methylthiazolium iodide; P450, cytochrome P450; rR, resonance Raman; SVD, singular value decomposition.

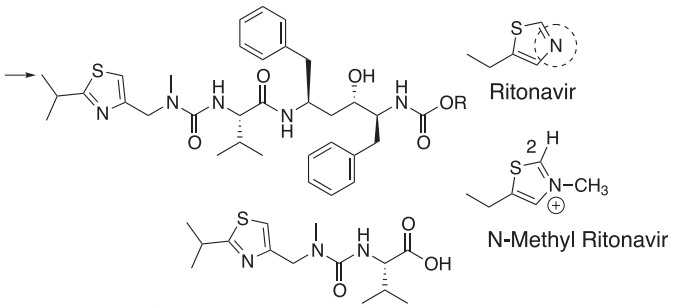

Fig. 1. Structures of ritonavir, NMeR, and MITV. The CYP3A4 heme-coordinating nitrogen atom is highlighted with a dashed circle, and the site of hydroxylation is indicated with an arrow. The acidic C2 proton in NMeR is indicated as labeled.

polyhalogenated methanes has been attributed to ferrous dihalocarbene complexes (Wolf et al., 1977; Ruf et al., 1984). The methylenedioxphenyl substituent that is present in therapeutic drugs (i.e., paroxetine and tadalafil) (Ring et al., 2005), drugs of abuse (i.e., methylenedioxymethamphetamine) (Heydari et al., 2004), and insecticide synergists (i.e., piperonyl butoxide) (Casida, 1970) undergoes NADPH and O_2-dependent oxidation to generate the carbene methylenedioxyphenyl-2-ylidene (MDP), which strongly coordinates to the Fe^{2+}-heme iron and gives rise to a distinct split Soret band with maxima at ~427 and 455 nm (Hodgson and Philpot, 1974).

Our search for a high-affinity type I ligand led us to *N*-methylritonavir (NMeR, Fig. 1), an analog wherein the heme-coordinating thiazole nitrogen has been blocked by methylation. Herein, we report a detailed spectroscopic characterization of the NMeR complex with recombinant CYP3A4. UV-visible absorption and resonance Raman (rR) spectroscopy demonstrate that the spin-state populations of NMeR-CYP3A4 are strongly pH dependent. There is a substantial high-spin population at low pH that shifts to low spin at high pH. UV-visible difference spectra of the low-spin complexes have split Soret bands with a strongly red-shifted component similar to those observed in the spectra of carbene complexes. Recognizing the acidity of the C2 carbon of *N*-methylthiazolium ions, we propose that the hydrophobic environment of the CYP3A4 active site suppresses the pK_a of NMeR's *N*-methylthiazolium C2 hydrogen such that it is readily deprotonated to a *N*-methyl-1,3-thiazol-2-ylidene (thiazol-2-ylidene hereafter), an *N*-heterocyclic carbene that has high affinity for iron. Density functional theory calculations using a truncated model of the Fe^{3+}-P450 active site support this scenario. To our knowledge, this represents the first example of a transition metal-*N*-heterocyclic carbene complex within an enzyme.

Materials and Methods

Materials. NMeR bicarbonate and N-[2-Isopropylthiazol-4-ylmethyl(methyl)carbamoyl]-L-valine (MITV) were purchased from Toronto Research Chemicals (Toronto, Canada). 5-Aminolevulinic acid was purchased from Chem-Impex International (Wood Dale, IL), isopropyl β-D-1-thiogalactopyranoside from LabScientific (Highlands, NJ), and 3-[3-(cholamidopropyl)dimethylammonio]-1-propane (CHAPS) from AG Scientific (San Diego, CA). Chromatography columns were purchased from GE Healthcare Bio-Sciences (Pittsburgh, PA). All other reagents of the highest available grade were purchased from Sigma-Aldrich (St. Louis, MO) or Fisher Scientific (Pittsburgh, PA). *N*-methylthiazolium iodide (NMTI) was synthesized as previously described by Kena Diba et al. (2010). To a solution of thiazole (2 ml, 2.4 g, 28.2 mmol) in 6 ml of methanol, iodomethane (2.18 ml, 5 g, 35.2 mmol) was added, and the solution was stirred for 48 hours at room temperature in the dark. The resultant white crystals were vacuum filtered and washed with methanol followed by ethyl acetate. The crystals were dried under vacuum overnight to yield 2.05 g of NMTI (9.05 mmol, 32%). For mass spectrometry, the calculated value for C_4H_6NS [M^+] is 100.02 a.m.u., 100.04 a.m.u. was found.

CYP3A4 Expression and Purification. CYP3A4 lacking residues 3–23 and modified to have a C terminal 4×His tag was expressed in DH5α *Escherichia coli* cells using the pCW-CYP3A4 plasmid generated in our laboratory. We used 100 ng of pCW-CYP3A4 plasmid to transform chemically competent DH5α cells. Two colonies were used to inoculate 100 ml of terrific broth (100 μg/ml ampicillin), and they were grown for 16 hours at 37°C. One liter batches of terrific broth supplemented with 100 μg/ml ampicillin were inoculated with 20 ml of starter culture and grown at 200 rpm and 37°C until the o.d. at 600 nm reached 0.4–0.6. The incubation temperature was then decreased to 24°C until the o.d. reached 0.8 at which time the rotations were decreased to 150 rpm. The cultures were then supplemented with 0.5 mM of 5-aminolevulinic acid and induced with 1 mM isopropyl β-D-1-thiogalactopyranoside. After 24 hours the bacteria were harvested by centrifugation at 4000*g* for 10 minutes.

The cell pellets were resuspended (1.5 ml•g^{-1} cells) in lysis buffer (100 mM potassium phosphate, pH 7.4, 500 mM KCl, 0.5% CHAPS, 10% glycerol, and 2 mM β-mercaptoethanol). On ice, the resuspension was incubated for 45 minutes with lysozyme (1.5 mg/ml) and subsequently sonicated for 15 minutes. The insoluble material was pelleted by centrifugation at 30,000*g* for 1 hour. The supernatant was loaded onto a Ni^{2+}-NTA column pre-equilibrated with wash buffer (100 mM potassium phosphate, pH 7.4, 500 mM KCl, 0.2% CHAPS, 20 mM imidazole 10% glycerol, and 2 mM β-mercaptoethanol). The column was washed with 15 column volumes of wash buffer and eluted with elution buffer (100 mM potassium phosphate, pH 7.4, 500 mM KCl, 0.2% CHAPS, 100 mM imidazole 10% glycerol, 2 mM β-mercaptoethanol).

Red-colored fractions were pooled and exchanged into dilution buffer (25 mM potassium phosphate, pH 6.8, 10% glycerol, and 2 mM β-mercaptoethanol) with several rounds of concentration and dilution using Amicon centrifugal concentrators (MWCO 30 kDa). Buffer-exchanged protein was then loaded onto a CM-Sepharose column equilibrated in dilution buffer. CYP3A4 was subsequently eluted with a linear gradient of 0 to 500 mM KCl in dilution buffer. Fractions with an A_{417}/A_{280} ratio >1.3 were pooled and dialyzed into storage buffer (50 mM potassium phosphate, pH 7.4, 50 mM KCl, 20% glycerol, and 2 mM β-mercaptoethanol) and stored at −80°C until required.

UV-Visible Absorbance Analysis of Ligand Binding. Measurement of UV-visible absorbance spectra was performed on a dual-beam Olis Cary-14 Spectrophotometer Conversion (Olis, Bogart, GA). Samples of purified CYP3A4 in 25 mM bis-tris propane/25 mM bicine buffer (pH 6.4–8.4) containing 50 mM KCl, 0.1 mM EDTA, and 20% glycerol were split equally into two cuvettes, and difference spectra (300–700 nm) were collected after a baseline and after the addition of ligands dissolved in dimethylsulfoxide (DMSO). Samples were allowed to equilibrate for 15 minutes after the addition of each aliquot before recording the spectra. The final volume of DMSO did not exceed 1% of the total sample volume.

Due to the extreme variation in the absorbance minima and maxima in difference spectra with pH, particularly when NMeR is present, an approach based on singular-value decomposition (SVD) (Henry and Hofrichter, 1992) was applied to determine the dissociation constants from sets of spectra generated by the ligand titrations. Spectra for each ligand concentration (n) were arranged in columns of

a data matrix $[A(\lambda,n)]$ and subjected to the SVD method that decomposes the data matrix into the product of matrices $A = USV^T$. After SVD analyses of the raw data, spectra were reconstructed using a set of truncated matrices, wherein only the first column vectors from each of U, S, and V^T derived from the raw spectra were retained while the remaining matrix elements were set to zero, thereby removing the experimental noise partitioned into those elements.

In turn, the spectral amplitudes $a = SV^T$ calculated using the truncated matrices were used to determine dissociation constants, K_d, by fitting the first column vector of a to the corresponding total ligand concentrations $[L_t]$ by minimizing

$$f(a,[L_t],[E]) = a - \frac{a_{\max}[L_f]}{K_d + [L_f]} \quad (1)$$

using *fsolve* in MATLAB, where $[L_f] = [L_t] - \frac{[E]a}{a_m}$ is the concentration of free ligand, $a_{\max}$ is the spectral amplitude at ligand saturation, and $[E]$ is the enzyme concentration. In the case of ritonavir, the spectral amplitudes were better described by the cooperative model

$$a = \frac{a_{\max}[L_t]^n}{K_d^n + [L_t]^n} \quad (2),$$

where n is the Hill coefficient.

The effects of oxidation and reduction on the difference spectra were performed using potassium hexachloroiridate and sodium dithionite, respectively. In the oxidation experiments, samples containing 3–5 μM CYP3A4 and 200 μM NMeR were prepared and allowed to equilibrate as described previously for the ligand titrations. After equilibration of the samples in the spectrophotometer, potassium hexachloroiridate was added to a final concentration of 50 μM, and the spectra were recorded every 5 minutes for 2.5 hours. For reduction experiments, 1.5 μM CYP3A4 samples (1 ml) in buffer (pH 7.4) were purged with N_2 and split equally between two cuvettes. We added 200 μM NMeR to the first cuvette and an equal amount of DMSO to the second cuvette, and both were allowed to equilibrate for 15 minutes. A baseline spectrum was measured with NMeR-Fe^{3+}-CYP3A4 and Fe^{3+}-CYP3A4 in the sample and the reference positions of the spectrophotometer, respectively. To measure the NMeR-Fe^{2+}-CYP3A4/Fe^{2+}-CYP3A4 difference spectrum, equal volumes of a saturated solution of sodium dithionite were added to each cuvette, and the spectra were repeatedly measured over several minutes until the spectrum stabilized.

Resonance Raman Spectroscopy. The rR spectra were obtained after excitation with the 406.7 nm line of a Coherent Innova 302C krypton ion laser (Coherent, Santa Clara, CA). Laser powers at the sample were 35 mW. Samples (100–200 μl) were maintained in spinning NMR tubes during data collection. Spectra were collected using a f/9.7 single-grating monochromator (Acton SP2750; Princeton Instruments, Trenton, NJ) with a 100 μm slit width, using 2400 grooves/mm gratings, and were imaged using a 1340 × 400 pixel back-illuminated charge-coupled device camera with UV optimized coatings (PyLoN 400BR eXcelon; Princeton Instruments). The reported spectra are the mean of three 10-minute scans and are unsmoothed. Reference calibrations were performed with respect to a mercury vapor lamp. The nonlinear fluorescence background of rR spectra were removed using asymmetric least squares in MATLAB (http://zanran_storage.s3.amazonaws.com/www.science.uva.nl/ContentPages/443199618.pdf).

The concentrations of CYP3A4 were ~8 μM in 25 mM bis-tris propane/25 mM bicine buffer (pH 6.0–8.4) containing 50 mM KCl, 0.1 mM EDTA, and no ligand, 200 μM NMeR, or 200 μM ritonavir. To determine the relative populations of the high- and low-spin CYP3A4 from the corresponding positions of the ν_3 bands in the spectra, these were fit to Gaussian line shapes, and their intensities were calculated by numeric integration. Calculation of the percentage of the enzyme populations in the high-spin configuration (%HS) were computed using the equation $\%HS = (100I^{HS})/(RI^{IS} + I^{HS})$, where $R = 1.24$ is the intensity ratio determined by Mak et al. (2013) for CYP3A4 to account for differences in the Raman cross-sections of the ν_3 band in the high- and low-spin states.

Density Functional Theory Calculations. A truncated model consisting of a pristine iron porphyrin and a thiolate (HS^-) ligand was used to model the essential elements of ligand coordination to the P450 heme. The energetics of the reaction to replace water by several azaheterocycles and MDP were computed using density functional theory. Geometry optimizations and vibrational frequency analyses were performed using the M06 density functional (Zhao and Truhlar, 2008) and def2-TZVP (Weigend and Ahlrichs, 2005) basis sets with the Gaussian 09 suite of programs (Gaussian, Wallingford, CT). Calculations using the B3LYP density functional (Becke, 1988, 1993a,b) including the D3 dispersion correction (Grimme et al., 2011) and def2-TZVP basis set were performed using the Turbomole 6.3 suite of programs (Ahlrichs et al., 1989). All reported energies include zero-point energy corrections derived from harmonic vibrational frequency analyses. Vertical excitation energies were performed with time-dependent density functional theory using the TPSSh (Tao et al., 2003) functional, def2-TZVPP basis sets, RI-J COSX approximation (Neese et al., 2009), and the M06/def2-TZVP optimized geometries with the ORCA 3.02 program (Neese, 2012).

Results

UV-Visible Absorbance Analysis of Ligand Binding. In the crystal structure of CYP3A4 bound to ritonavir, the thiazole nitrogen is clearly coordinated to the heme iron, and its titration into the enzyme results in a type II difference spectrum (Sevrioukova and Poulos, 2010). Hence, we expected that methylating the nitrogen ligand would disrupt coordination and facilitate displacement of the bound water to induce a high-spin transition (Fig. 2, A–C). To our surprise, the addition of NMeR at pH 7.4 shifts the Soret band of CYP3A4 to 421 nm like that observed for ritonavir (Sevrioukova and Poulos, 2010) (Fig. 3A). Recognizing the acidity of the *N*-methylthiazolium C2 proton(Breslow, 1958), we considered the possibility that this proton in NMeR could likewise be deprotonated to the corresponding thiazol-2-ylidene, which in turn could replace water as the sixth axial ligand (Fig. 2, A→B→D). To test this hypothesis, the UV-visible spectra of CYP3A4 were measured at pH 6.0, 6.4, 7.0. 7.4, 8.0, and 8.4 in a mixed bis-tris propane/bicine buffer to maintain uniform buffering capacity across this range (Fig. 3A). At pH 6.0, the Soret band maximum is at 418 nm, consistent with the presence of the low-spin, Fe^{3+}-H_2O enzyme. However, there is a distinct shoulder present at 390 nm and a weak band at 637 nm, both consistent with an admixture of the penta-coordinate, high-spin state of the enzyme, as initially expected. As the pH is incrementally increased, the 390 nm component of the Soret and the 637 nm bands disappear. At pH 8.4, the high-spin features of the spectrum are no longer visible, and the Soret band maximum has shifted to 422 nm. The dramatic changes in these spectral features support a pH-dependent change in the NMeR-CYP3A4 interaction.

Difference spectra of NMeR at pH 6.4, 7.4, and 8.4 were measured to determine the binding affinities and identify any unique distinguishing features in the spectra (Fig. 4, A–C). At pH 6.4, titration of NMeR into CYP3A4 results in a classic type I spectrum with a maximum at 382 nm and minimum at 412 nm. Repetition of the titration experiment at pH 7.4 results in a difference spectrum with a distinct split-Soret

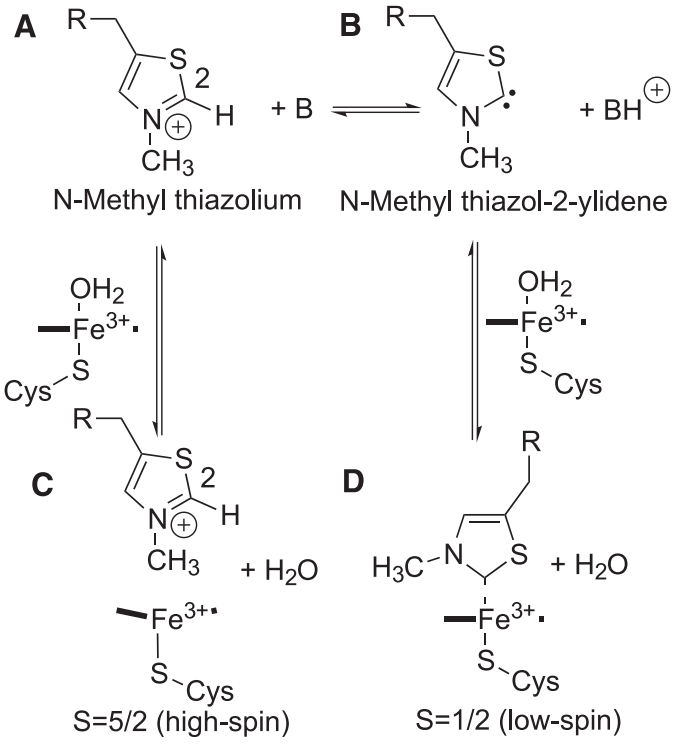

Fig. 2. Putative proton-dependent equilibrium between (A) the *N*-methylthiazolium unit and (B) thiazol-2-ylidene. (C) The *N*-methylthiazolium is expected to bind above the heme plane, displace the coordinated water molecule, and induce a low- to high-spin transition of the heme iron. (D) Thiazol-2-ylidene is a Lewis base that replaces the water ligand to form a hexa-coordinate low-spin complex.

band, which has maxima at 373, 433, and 467 nm and a minimum at 412 nm. At pH 8.4, the 467 nm maximum and 412 nm minimum are retained while the remaining maxima shift to 432 nm and 369 nm. Because the extrema of the difference spectra change dramatically between pH 6.4 and 7.4, the method relying on SVD with fitting of the spectral amplitudes to determine K_d values was used. The K_d values for NMeR are likewise pH dependent, undergoing a 14-fold decrease between pH 6.4 and 8.4. These observations support the increased contribution of a strong stabilizing component of the CYP3A4-NMeR interaction with increasing pH.

To determine whether the UV-visible spectral changes and K_d decrease observed with NMeR were the result of pH effects on the protein, a parallel set of titrations and difference spectra were measured with ritonavir (Fig. 4, D–F). In the Soret region, all spectra have troughs and peaks at 407 nm and 426 nm, respectively. In the α/β region, peaks were consistently identified at 544 nm and 584 nm, with a trough at 568 nm. Unlike the other ligands investigated in this study, the spectral amplitudes fit poorly to a single-binding site model. Alternatively, these data were best described by the Hill cooperative model. Within the reported error, the K_d values determined at pH 6.4 and 7.4 were the same (0.45 μM and 0.42 μM), while this value slightly decreased at pH 8.4 (0.32 μM). Furthermore, ritonavir binding was similarly positively cooperative in each of these experimental conditions.

The crystal structure of the ritonavir-CYP3A4 complex clearly illustrates the coordination of the thiazole fragment to the CYP3A4 heme iron. Nevertheless, we sought to

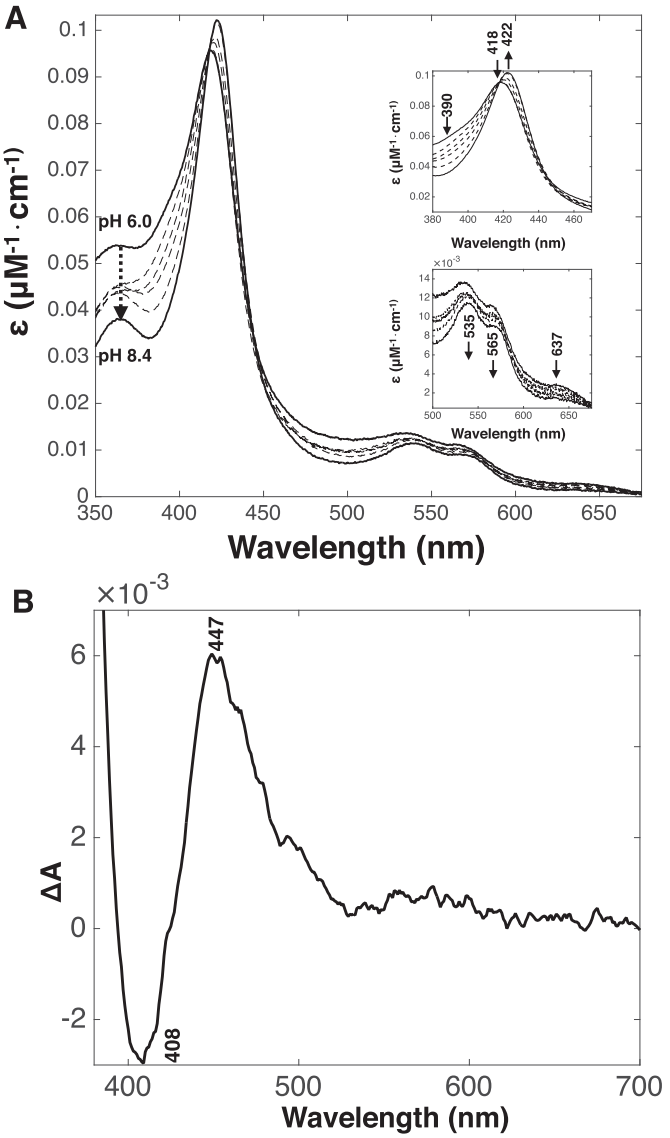

Fig. 3. (A) UV-visible absorption spectra of Fe^{3+}-CYP3A4 (2 μM) in the presence of 200 μM NMeR at pH 6.0, 6.4, 7.0, 7.4, 8.0, and 8.4. The Soret and α/β bands are in insets. (B) Representative Fe^{2+}-CYP3A4-NMeR/Fe^{2+}-CYP3A4 difference spectrum. Samples contained 1.5 μM CYP3A4 and 200 μM NMeR.

determine whether the observed UV-visible spectra could alone be attributed to the interaction of this heterocycle or whether the interactions with the remainder of the ritonavir molecule tuned the spectra of the complex. Indeed, the Soret and α/β regions of the thiazole-CYP3A4 spectra are identical to that of the ritonavir complex, supporting that the ritonavir scaffold does not influence the spectrum (Supplemental Fig. 2). The K_d of thiazole is 3.4 $\pm$ 1.0 mM at pH 7.4, more than 4800-fold higher than that measured for ritonavir. Additionally, the K_d of thiazole is nearly one and two orders of magnitude higher than the K_d values measured for 1,2,4-triazole and imidazole (Conner et al., 2012), and, as supported by density functional theory calculations, it is among the weakest azaheterocyclic ligands for thiolate-ligated Fe^{3+}-heme.

NMTI was synthesized and titrated into the CYP3A4 to lend further support to the concept that the unique features of the

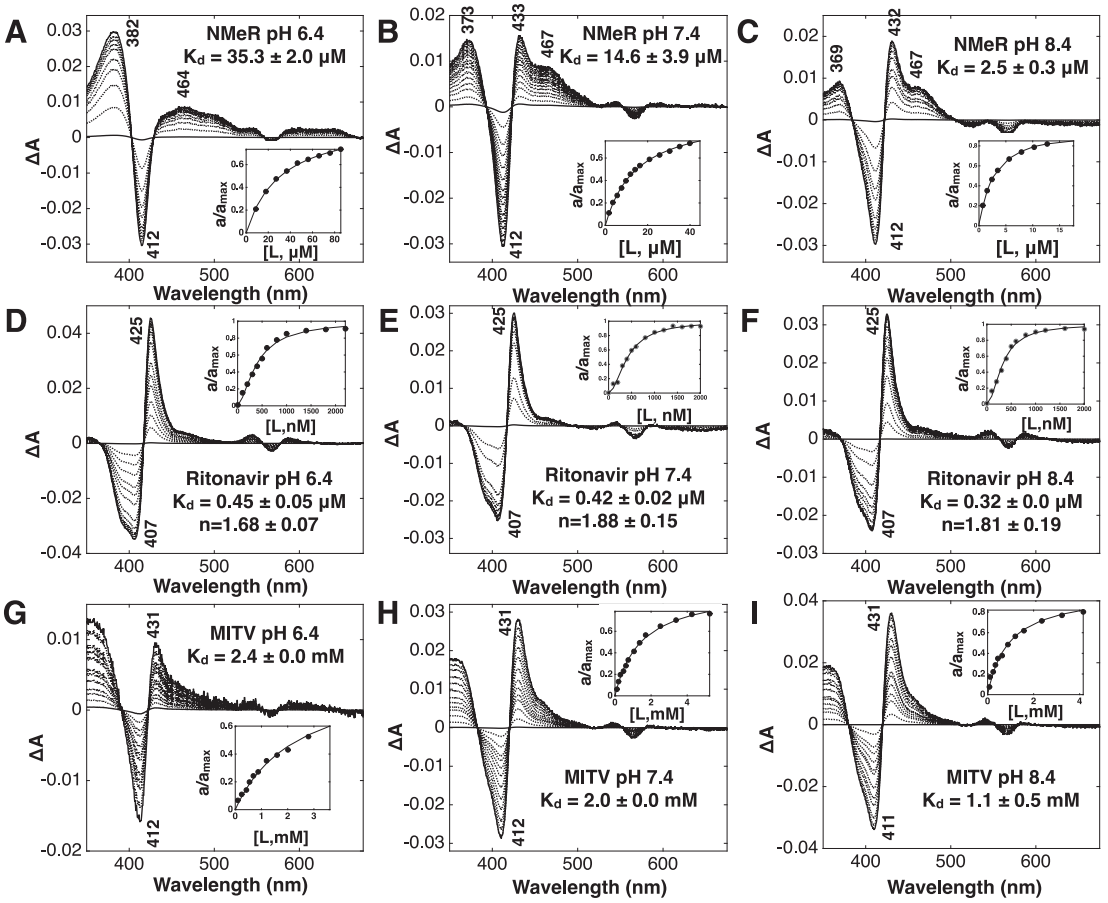

Fig. 4. CYP3A4 (2 μM) absorbance difference spectra and binding isotherms (inset) for (A–C) NMeR, (D–F) ritonavir, and (G–I) MITV, each at pH 6.4, 7.4, and 8.4 (left to right). Reported K_d values and Hill coefficients for ritonavir are the mean of three ligand titration experiments ± S.D. Inset binding isotherms illustrate data from a single representative titration experiment with the corresponding data fitting. Spectra of MITV in buffer show that the strong band at 360 nm is attributable to the ligand and not the complex with CYP3A4.

difference spectra were attributed to the deprotonation and coordination of the *N*-methylthiazolium unit of NMeR. NMTI did not produce difference spectra with the conditions used for NMeR. However, incubation of 20 mM NMTI with 4 μM CYP3A4 at pH 8.4 over 2.5 hours resulted in a difference spectra having a split Soret band with maxima at 378 nm and 464 nm, similar to the features obtained with NMeR (Supplemental Fig. 1). This result both underscores the importance of the ritonavir scaffold to achieve reasonable binding affinity and supports the notion that the *N*-methylthiazolium fragment contributes the unusual spectral features to the NMeR-CYP3A4 complex.

Crystal structures clearly demonstrate that analogs of ritonavir lacking the phenyl side chains maintain the "thiazole-first" binding mode. In cases when the thiazole has been replaced with another azaheterocycle, coordination is generally maintained. Additionally, in examples wherein the azaheterocycle is absent, the orientation of the remaining scaffold remains consistent with that of ritonavir (Sevrioukova and Poulos, 2012, 2013; Kaur et al., 2015). Moreover, the observation that deaza-ritonavir (the heme coordinating nitrogen is replaced by C-H) produces a partial type I spectral change is similarly consistent with "thiazole-first" binding. Hence, evidence supports that the "thiazole-first" binding mode is very tolerant to scaffold changes, and we therefore expected NMeR to assume a similar orientation in the active site.

Nevertheless, we sought to investigate the possibility that pH change partially inverts NMeR's binding mode such that the isopropyl unit is oriented toward the heme iron and that this scenario could underlie the unusual features of the difference spectra. To test this hypothesis, titration experiments were performed with MITV (Fig. 1), a truncated analog of ritonavir representing only the left-hand side of the molecule and lacking the heme-coordinating thiazole. MITV should only produce type II spectra if the isopropyl thiazole fragment interacts with the CYP3A4 heme, so it was used as a tool to investigate the pH dependence of isopropyl thiazole fragment coordination.

As illustrated in Fig. 4, G–I, the features of the difference spectra are pH-independent, and they lack the distinctive 467 nm band observed in NMeR difference spectra. Furthermore, MITV is a comparatively weak ligand for CYP3A4 (K_d = 1.1–2.4 mM) and exhibits only a 2-fold decrease in K_d with increasing pH. These differences preclude the possibility that the unusual difference spectra are the result of pH-dependent NMeR inversion in the CYP3A4 active site.

The strongly red-shifted component at 467 nm is a characteristic typically observed in the spectra of Fe^{2+}-carbene complexes (Hodgson and Philpot, 1974; Wolf et al.,

1977; Ruf et al., 1984). Although there is no obvious electron source capable of reducing the Fe^{3+}-thiazol-2-ylidene in Fig. 2D to a Fe^{2+}-thiazol-2-ylidene species under the present experimental conditions, the spectra of the NMeR -CYP3A4 complex was treated with both oxidizing and reducing agents with the expectation that spectral changes would provide insight into the dominant iron oxidation state before treatment with these reagents. In the presence of the reducing agent sodium dithionite, the Fe^{2+}-NMeR-CYP3A4/Fe^{2+}-CYP3A4 difference spectra revealed notable changes. Spectra of the reduced species (Fig. 3B) displayed a prominent Soret band at 447 nm. Conversely, measurement of difference spectra in the presence of the strong oxidant potassium hexachloroiridate did not reveal any changes in the difference spectra with the exception of moderate increases in the intensities of the 433 nm and 467 nm bands over 3 hours. However, an equivalent increase was likewise observed in the control experiments lacking potassium hexachloroiridate. The observation that the CYP3A4-NMeR complex is readily reduced to a spectroscopically distinct species, possibly the corresponding to Fe^{2+}-CYP3A4-NMeR complex, while being resistant to a strong one-electron oxidant supports that the CYP3A4-NMeR complex is a Fe^{3+}-carbene complex.

Resonance Raman Spectroscopy of CYP3A4. Resonance Raman spectroscopy permits measurement of the symmetry-allowed vibrational transitions of the heme chromophore in the P450 active site environment. Because the vibrational manifold is sensitive to changes in electronic structure and conformation of the heme, we have used this approach to interrogate the effects of pH and ligand binding on these characteristics of the CYP3A4 active site. To this end, rR spectra of ligand-free CYP3A4 as well as the ritonavir and NMeR complexes were measured (Fig. 5).

The high-frequency regions of CYP3A4 rR spectra are illustrated in Fig. 5, A–C. The oxidation-state sensitive marker bands (ν_4) are positioned at 1374 cm^{-1} in all spectra regardless of pH or ligand and are consistent with the Fe^{3+} state of the heme in these experiments. Spin-state sensitive bands in the spectra of ligand-free CYP3A4 occur at 1502 cm^{-1} (ν_3), 1584 cm^{-1} (ν_2), and 1638 cm^{-1} (ν_{10}), all of which are consistent with a predominately low-spin Fe^{3+}-H_2O enzyme. In the penta-coordinate high-spin state, these markers are expected to shift to ~1490 cm^{-1} (ν_3), ~1570 cm^{-1} (ν_2), and ~1630 cm^{-1} (ν_{10}). Due to its minimal overlap with other bands in the spectra, the intensity of ν_3 is routinely used to determine the relative contributions of the spin states. In the ligand-free enzyme, a high-spin component of ν_3 is represented as a small shoulder 1490 cm^{-1}. Fitting of the high- and low-spin components of the bands to two Gaussians and determination of their relative intensities reveal only a small pH-dependent variation from 8.6% ± 0.5% at pH 6.0 to 3.6% ± 0.5% at pH 8.4. At pH 7.4, the high-spin contribution was determined to be 4.9% ± 0.5%, in agreement with the 5% contribution previously determined for the ligand-free enzyme (Mak et al., 2013). The remaining rR spectral features nearly overlap over the entire pH range, supporting that these changes do not appreciably influence the heme or its immediate environment.

At pH 6.0, NMeR-bound CYP3A4 has strong contributions from the high-spin marker bands at 1489 cm^{-1} (ν_3), 1569 cm^{-1} (ν_2), and 1632 cm^{-1} (ν_{10}). As the pH increases, their intensities decrease, and they coalesce into their corresponding low-spin components. Focusing on ν_3 to quantitate the contributions of each spin state, the high-spin contribution was found to be maximal at pH 6.0 (30.5% ± 0.5%), decreasing with the increasing pH to a minimum at pH 8.4 (4.3% ± 0.5%).

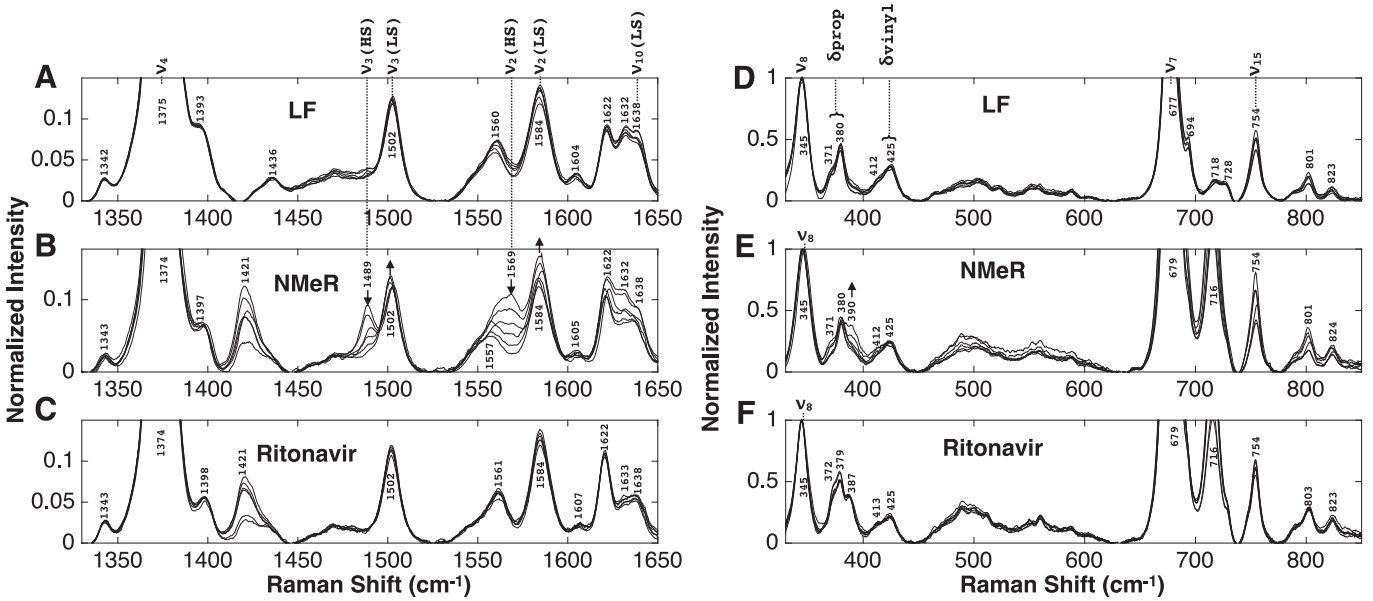

Fig. 5. The rR spectra of (A, D) ligand-free, (B, E) NMeR-bound, and (C, F) ritonavir-bound Fe^{3+}-CYP3A4 at pH 6.0, 6.4, 7.0, 7.4, 8.0, and 8.4. The high- and low-frequency regions are illustrated in panels A–C and D–F, respectively. Protein concentrations were 8–10 μM and those of NMeR and ritonavir were 200 μM. The high- and low- frequency spectra were normalized to the intensities of the ν_4 and ν_8 bands, respectively. Bands at 721 cm^{-1} and 1421 cm^{-1} are present in samples containing ligands alone (without CYP3A4) and are therefore not attributable to the CYP3A4-NMeR or CYP3A4-ritonavir complexes. Arrows indicate the direction of the intensity changes occurring in relevant bands with increasing pH.

Nonlinear least-squares fitting of the %HS and pH values to the equation

$$\%HS = \frac{\%HS_{\min} - (\%HS_{\max} - \%HS_{\min})}{1 - 10^{pH - pK_a}} \quad (3)$$

resulted in an apparent pK_a of 7.4 for the high- to low-spin transition (Fig. 6). In contrast to NMeR, features of the rR spectra with ritonavir are resistant to changes in pH, and they indicate that the high-spin content does not exceed 3%. Considering the pH resistance of rR spectra of the ligand-free and ritonavir-bound enzymes and the near identical chemical structures of these ligands, it appears that the observed pH dependence of the spin shift with NMeR is attributable to its *N*-methylthazolium unit. Hence, the apparent pK_a of 7.4 is tentatively assigned to the NMeR C2 proton, and the loss of the high-spin enzyme is attributed to capture of the thiazol-2-ylidene by the CYP3A4 heme.

The corresponding low-frequency regions of the rR spectra are illustrated in Fig. 5, D–F. Spectra of the ligand-free and ritonavir-bound enzymes are similarly resistant to changes in pH. Furthermore, their spectra are very similar with the exception of the so-called propionate bands, which generally have components positioned at ~370 cm^{-1}, ~380 cm^{-1}, and ~390 cm^{-1}. The positions of these bands can be affected by changes in interactions between the propionates and the protein, but recent evidence obtained with hemes containing isotopically-labeled methyl groups support that these modes are more adequately characterized as out-of-plane distortions of the heme C and D pyrroles (Mak et al., 2004; Podstawka et al., 2006). The propionates envelope of the ligand-free enzyme has bands positioned at 371 cm^{-1} and 380 cm^{-1}. These plus an additional band at 387 cm^{-1} appear in spectra of the ritonavir-bound enzyme.

A similar band positioned at 390 cm^{-1} also appears in the spectra of the NMeR complex, although its intensity is pH dependent. Because this band consistently appears in the ritonavir spectra and is pH dependent in NMeR spectra, we speculate that this increase in Raman activity is caused by a conformational change in the propionates and/or the C/D rings of the heme that accompanies coordination by the ligand.

Density Functional Theory Calculations. To assess the geometries and strength of the iron-carbon bond formed between the thiazol-2-ylidene and the P450 heme relative to other azaheterocyles and MDP, we used density functional theory calculations employing the B3LYP-D3 and M06 density functionals. The former functional was selected because it has been widely applied to study P450 chemistry (Shaik et al., 2005, 2010); the latter was selected for its improved performance for the treatment of transition metal complexes (Cramer and Truhlar, 2009).

The geometry of a model thiazol-2-ylidene coordinated to the ferric iron of our truncated model optimized at the M06/def-TZVP level of theory is illustrated in Fig. 7. Both density functionals predict a stable, low-spin (S = 1/2) complex with the Fe-C and Fe-S bond lengths comparable to the corresponding Fe-N (~2.1 Å) and Fe-S (~2.3 Å) bond lengths observed in high-resolution crystal structures of P450-imidazole complexes (Verras et al., 2006; Sugimoto et al., 2008). Attempts to optimize the geometry of a complex with the sulfur atom coordinated to the iron atom resulted in dissociation of the complex. Geometry optimizations at both levels of theory with other azaheterocycles (Table 1) predict that these distances vary at most by ~0.06 Å. However, the Fe-C bond in the MDP complex is notably shorter by 0.05–0.10 Å compared with those predicted for the azaheterocycle complexes.

In an effort to determine the relative binding energy of the thiazol-2-ylidene in comparison with other azaheterocyles and MDP, energy changes for displacement of H_2O from a low-spin

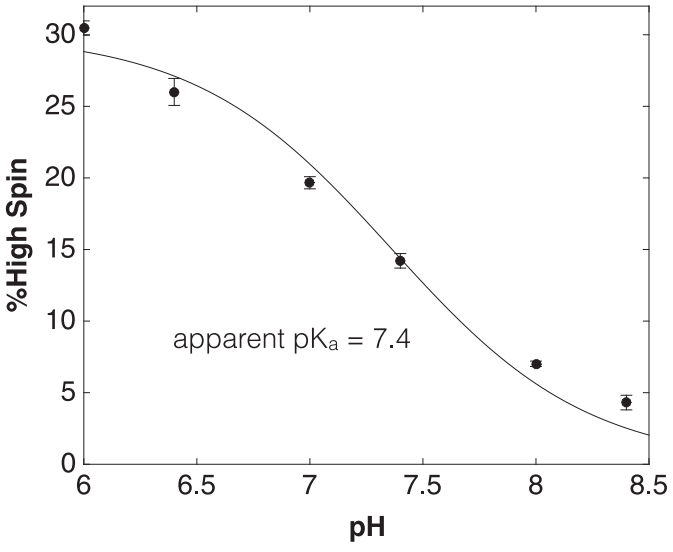

Fig. 6. Titration curve illustrating the pH-dependence of spin-state in NMeR bound CYP3A4 derived from the ν_3 bands of rR spectra.

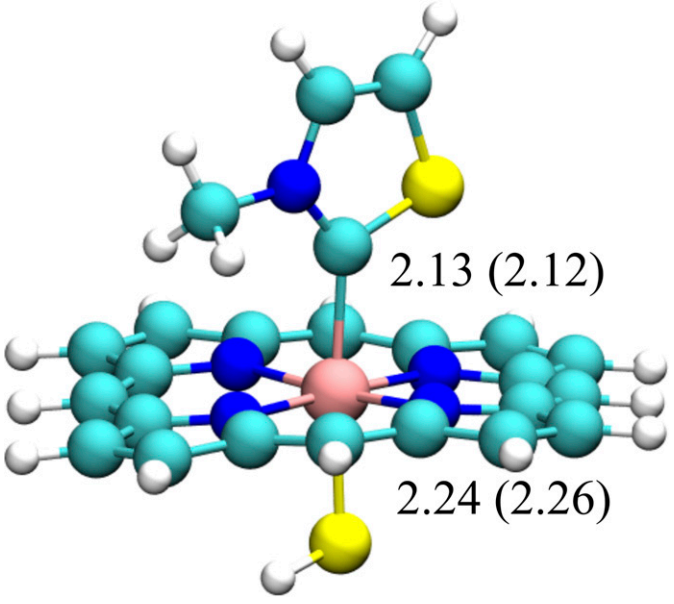

Fig. 7. M06/def2-TZVP optimized geometry of the [(Porphyrin^{2-})(Fe^{3+})(HS^-)(*N*-methyl thiazol-2-ylidene)] complex. The Fe-C2 and Fe-S distances are labeled in Angstroms. Distances of the complex optimized at the B3LYP-D3/def2-TZVP level of theory are in parentheses.

TABLE 1
Density functional theory energetics (kcal•mol^{-1}) for replacement of water as the proximal ligand in a truncated model of the P450 active site by several heterocycles and relevant bond distances in the complexes

Ligand (X)	M06/def2-TZVP			B3LYP-D3/def2-TZVP		
	ΔE	Fe-X	Fe-S	ΔE	Fe-X	Fe-S
Thiazol-2-ylidene	−16.1	2.13	2.24	−15.4	2.12	2.26
1,2,4-Triazole (N2)	−15.2	2.10	2.21	−14.0	2.12	2.22
1,2,4-Triazole (N4)	−14.8	2.11	2.21	−13.6	2.11	2.22
Methylenedioxyphenyl-2-ylidene	−10.7	2.05	2.23	−10.3	2.00	2.24
Imidazole	−10.3	2.10	2.22	−9.8	2.10	2.23
Pyridine	−8.5	2.17	2.22	−9.0	2.16	2.22
1,2,3-Triazole (N2)	−6.9	2.11	2.21	−6.6	2.14	2.21
1,2,3-Triazole (N1)	−6.4	2.13	2.21	−5.4	2.13	2.22
Thiazole	−4.6	2.16	2.21	−7.5	2.13	2.22

H_2O-coordinated model were calculated for each of the respective fragments:

$$\left[(Porphyrin^{2-})(Fe^{3+})(HS^{-})(H_2O)\right] + L \rightarrow \left[(Porphyrin^{2-})(Fe^{3+})(HS^{-})(L)\right] + H_2O \quad (4)$$

Displacement of H_2O by the fragments is consistently exothermic. With the exception of water displacement by N1 of 1,2,3-triazole and thiazole, the predicted energetic trends are the same for both the M06 and B3LYP-D3 functionals. Taking the magnitude of the exothermicity as an index of ligand strength, the trend follows as: thiazol-2-ylidene > 1,2,4-triazole > MDP > imidazole > 1,2,3-triazole > thiazole. These results differ in some respects to those described by Conner et al. (2012) whose study evaluated the energetics of water exchange by imidazole, 1,2,4-triazole, and 1,2,3 triazole using an identical model system, M06 functional, and the spin-state corrected 6-31G basis set (Swart et al., 2010). This study reported the energetic trend: imidazole (−5.3 kcal·mol^{-1}) > 1,2,4-triazole (−3.2 kcal·mol^{-1}) > 1,2,3 triazole-N2 (−2.8 kcal·mol^{-1}) > 1,2,3 triazole-N1 (−1.7 kcal·mol^{-1}). Notable differences between our results and those described in Conner et al. (2012) include the 2- to 5-fold differences in exothermicities as well as the prediction that coordination of imidazole is more exothermic than 1,2,4-triazole.

We speculate that these differences are attributable to the moderately-sized basis set used in their calculations. Owing to our use of a larger, more flexible basis set in these studies as well as the close agreement between the results obtained with two density functionals with different theoretical underpinnings, we are confident that our calculations are more reliable. Nonetheless, these calculations support the idea that, of the fragments that frequently occur in type II inhibitors of P450 enzymes, thiazol-2-ylidene is among the strongest ligands for Fe^{3+}-P450, closely followed by the two possible binding modes of 1,2,4-triazole.

To complement experimental evidence that NMeR binding to CYP3A4 results in a thiazol-2-ylidene complex, we used time-dependent density functional theory calculations to predict vertical excitation energies and oscillator strengths (*f*) that are comparable to experimental UV-visible absorption spectra. To confirm the validity of this approach, calculations were initially performed using models of systems with extensively documented UV-visible spectra. Specifically, we calculated the vertical excitation energies and oscillator strengths of the Fe^{2+}-CO and Fe^{2+}-MDP model systems. The Fe^{2+}-CO complex was predicted to have a strong Soret band at 448.7 nm ($f = 0.0126$), whereas the Fe^{2+}-MDP was predicted to have two nearly degenerate bands in the Soret region at 454.3 nm ($f = 0.0229$) and 454.6 nm ($f = 0.0230$). These predictions are in excellent agreement with the measured spectra of the synthetic complexes [(Fe^{2+})(PPIX^{2-})(CH_3S^{1-})(CO)] and [(Fe^{2+})(TPP^{2-})(nBuS^{1-})(MDP)] that have Soret bands at 450 nm and 459 nm, respectively (Collman and Sorrell, 1975; Mansuy et al., 1979). Recognizing the accuracy of the approach for these systems, we applied it to the Fe^{3+}-thiazol-2-ylidene complex. Vertical excitations of 430.4 nm ($f = 0.0026$) and 461.5 nm ($f = 0.0010$) were predicted, consistent with those observed in the NMeR-Fe^{3+}-CYP3A4 spectra.

Discussion

Herein we describe a detailed spectroscopic investigation of the complex between an *N*-methylthiazolium analog of ritonavir and CYP3A4. Despite the obstruction of the heme-coordinating nitrogen atom by methylation, it fails to consistently produce UV-visible spectra demonstrative of the expected high-spin transition of the heme iron. In view of the acidity of the *N*-methylthiazolium C2 proton and the sensitivity of its pK_a to environment, we executed variable-pH spectroscopy studies. Difference spectra confirmed that the contribution of the high-spin enzyme decreases with increasing pH, having definitively type I characteristics at pH 6.4 and split Soret bands at pH ≥7.4 that include a red-shifted component at 467 nm. The red-shifted component is similar to those observed in "metabolic intermediate complexes" that result from the bioactivation of dihalomethanes and methylenedioxyphenyl compounds to carbenes (Hodgson and Philpot, 1974; Wolf et al., 1977; Ruf et al., 1984). Changes in UV-visible spectra are accompanied by an increase in the affinity of NMeR for CYP3A4, indicative of further stabilization of the interaction under these conditions. Although the affinity of NMTI for CYP3A4 was too low to be measured by difference spectroscopy, extended incubations with large concentrations at high pH likewise produced spectra with the distinct red-shifted band observed in the NMeR-CYP3A4 complex, supporting that this fragment constitutes the heme-coordinating element. Conversely, variable pH difference spectroscopy demonstrated that changes in this condition do not appreciably affect the binding affinities or characteristics of the spectra

obtained with the closely related compounds ritonavir or MITV.

Taken together with the established acidity of the *N*-methylthiazolium C2 proton, these data point to the possibility that this fragment is deprotonated to a thiazol-2-ylidene, an *N*-heterocyclic carbene that in turn coordinates to the heme iron and is responsible for the unusual difference spectra. Density functional theory calculations using a minimal model of the putative thiazol-2-ylidene complex, [(Fe^{3+})(Porphyrin^{2-})(HS^{1-})(thiazol-2-ylidene)], revealed that it is indeed stable and that electronic excitation energies calculated using time-dependent density functional theory are in excellent agreement with UV-visible spectra of the NMeR-bound CYP3A4. This remarkable agreement bolsters the assignment of this interaction as a thiazol-2-ylidene-coordinated heme and supports that the unusual spectra are directly attributable to electronic transitions of the heme and this unusual ligand.

A more detailed view of the heme electronic structure and the influence of pH on its immediate environment was provided by rR spectroscopy. Only rR spectra of the NMeR-CYP3A4 complex demonstrated pH dependence, and only those bands corresponding to changes in spin state and out-of-plane distortions of the C/D pyrroles were affected. Because the binding mode of NMeR is expected to closely resemble that of ritonavir, whose rR spectra are not influenced by pH, these experiments likewise support that the pH-dependence is attributable to the *N*-methylthiazolium fragment. Hence, we tentatively assign the apparent pK_a of 7.4 to the NMeR C2 proton in the active site of CYP3A4. This value is at best an approximation of this pK_a for two reasons. First, the relative spin state contributions only provide an indirect measure of a protonation/deprotonation equilibrium. Second, the deprotonated species is readily captured by the heme and thereby distorts the equilibrium. Nevertheless, this pK_a is in line with the estimates made for the C2 proton in thiamine-dependent enzymes.

Deprotonation of an alkylthiazolium ion to a thiazol-2-ylidene likewise occurs in the catalytic cycles of thiamine-dependent enzymes. After the initial observation of Breslow (1958) that the C2 proton of *N*-methylthiazolium exchanges with D_2O with a half-life of 20 minutes, deprotonation of this position remains generally accepted as the initial step in thiamine-dependent catalysis. The first solution pK_a measurements of thiamine and *N*-methylthiazolium yielded values of 12.7 and $\geq$ 13.5, respectively (Hopmann and Brugnoni, 1973). Later measurements for thiamine assigned the C2 proton a pK_a of 18.0. Despite their high solution values, the active sites of these enzymes are known to suppress the C2 proton pK_a such that it is readily deprotonated under physiologic conditions. This idea is supported by the NMR studies of C2 deprotonation kinetics in pyruvate decarboxylase and transketolase, which showed that the protein environment accelerated these rates by as much as 2×10^5 (Kern et al., 1997). There is also evidence that pyruvate decarboxylase suppresses the pK_a of its enamine intermediate from 15.4 in water to ~6 in the enzyme environment, a change that corresponds to a billion-fold rate enhancement for enamine deprotonation (Jordan et al., 1999).

Spectroscopic measurements of thiazole and NMTI binding to the enzyme reveal they are very poor ligands, thus the high affinities of ritonavir and NMeR (at high pH) are conferred by hydrophobic interactions between the active site and the remaining ritonavir scaffold. Hence, for *N*-methylthiazolium to bind, the energetic destabilization resulting from placing a cation in the nonpolar environment must be offset by hydrophobic interactions between CYP3A4 and the scaffold. By compelling the *N*-methylthiazolium unit to enter this environment, the thermodynamic preference to accommodate the neutral thiazol-2-ylidene is enhanced and thereby drives the equilibrium toward deprotonation. This phenomenon is manifested as a measurable pK_a suppression.

Calculations support that the thiazol-2-ylidene interaction with the P450 heme is at least as strong as the azaheterocycles found in the tightest binding competitive inhibitors of P450s. Conversely, thiazole is predicted to be among the weakest ligands for the Fe^{3+}-P450. However, ritonavir binds to CYP3A4 with nearly 8-fold higher affinity at pH 8.4. This apparent discrepancy is logical for two reasons. First, because NMeR is a quaternary cation, there is a larger energetic penalty associated with stripping bound water molecules (desolvation) from the ligand before it enters the active site. Second, in ritonavir the thiazole N-atom is optimally positioned for coordination to the heme iron, although this is not the case for the C2 in NMeR. Hence, positioning of the C2 and accommodation of the methyl group likely coincide with a substantial rearrangement of this region relative to the binding mode observed for ritonavir, thereby adding to the energetic penalty. Indeed, NMeR is not an improvement over ritonavir with regard to affinity. However, it does demonstrate a novel carbene–P450 interaction that has the potential for optimization and possible applications in the development of inhibitors for CYP3A4 and other P450s. Finally, unlike other carbene ligands, oxidative or reductive bioactivation of the parent molecule is unnecessary to generate the iron-coordinating element.

Acknowledgments

The authors thank the Ohio Supercomputer Center for a generous allocation of computational resources.

Authorship Contributions

Participated in research design: Jennings, Hackett.
Conducted experiments: Jennings, Ritchie, Shock, Hackett.
Contributed new reagents or analytic tools: Lyons.
Performed data analysis: Jennings, Ritchie, Shock, Hackett.
Wrote or contributed to the writing of the manuscript: Jennings, Hackett.

References

Ahlrichs R, Baer M, Haeser M, Horn H, and Koelmel C (1989) Electronic structure calculations on workstation computers: the program system turbomole. *Chem Phys Lett* **162**:165–169.
Becke AD (1988) Density-functional exchange-energy approximation with correct asymptotic behavior. *Phys Rev A Gen Phys* **38**:3098–3100.
Becke AD (1993a) Density-functional thermochemistry. III. The role of exact exchange. *J Chem Phys* **98**:5648–5652.
Becke AD (1993b) A new mixing of Hartree–Fock and local density-functional theories. *J Chem Phys* **98**:1372–1377.
Breslow R (1958) On the mechanism of thiamine action. IV.1 Evidence from studies on model systems. *J Am Chem Soc* **80**:3719–3726.
Casida JE (1970) Mixed-function oxidase involvement in the biochemistry of insecticide synergists. *J Agric Food Chem* **18**:753–772.
Collman JP and Sorrell TN (1975) Letter: A model for the carbonyl adduct of ferrous cytochrome P450. *J Am Chem Soc* **97**:4133–4134.
Conner KP, Vennam P, Woods CM, Krzyaniak MD, Bowman MK, and Atkins WM (2012) 1,2,3-Triazole-heme interactions in cytochrome P450: functionally competent triazole-water-heme complexes. *Biochemistry* **51**:6441–6457.
Cramer CJ and Truhlar DG (2009) Density functional theory for transition metals and transition metal chemistry. *Phys Chem Chem Phys* **11**:10757–10816.
Denisov IG, Makris TM, Sligar SG, and Schlichting I (2005) Structure and chemistry of cytochrome P450. *Chem Rev* **105**:2253–2277.

Grimme S, Ehrlich S, and Goerigk L (2011) Effect of the damping function in dispersion corrected density functional theory. *J Comput Chem* **32**:1456–1465.
Guengerich FP (2001) Uncommon P450-catalyzed reactions. *Curr Drug Metab* **2**: 93–115.
Henry ER and Hofrichter J (1992) Singular value decomposition: application to analysis of experimental data. *Methods Enzymol* **210**:129–192 DOI:10.1016/0076-6879(92)10010-B.
Heydari A, Yeo KR, Lennard MS, Ellis SW, Tucker GT, and Rostami-Hodjegan A (2004) Mechanism-based inactivation of CYP2D6 by methylenedioxymethamphetamine. *Drug Metab Dispos* **32**:1213–1217.
Hirsch MS, Günthard HF, Schapiro JM, Brun-Vézinet F, Clotet B, Hammer SM, Johnson VA, Kuritzkes DR, Mellors JW, and Pillay D et al.; International AIDS Society-USA (2008) Antiretroviral drug resistance testing in adult HIV-1 infection: 2008 recommendations of an International AIDS Society-USA panel. *Top HIV Med* **16**:266–285.
Hodgson E and Philpot RM (1974) Interaction of methylenedioxyphenyl (1,3-benzodioxole) compounds with enzymes and their effects on mammals. *Drug Metab Rev* **3**:231–301.
Hollenberg PF (2002) Characteristics and common properties of inhibitors, inducers, and activators of CYP enzymes. *Drug Metab Rev* **34**:17–35.
Hopmann RF and Brugnoni GP (1973) pK of thiamine C(2)H. *Nat New Biol* **246**: 157–158.
Jordan F, Li H, and Brown A (1999) Remarkable stabilization of zwitterionic intermediates may account for a billion-fold rate acceleration by thiamin diphosphate-dependent decarboxylases. *Biochemistry* **38**:6369–6373.
Kaur P, Chamberlin R, Poulos TL, and Sevrioukova IF (2015) Structure-based inhibitor design for evaluation of a CYP3A4 pharmacophore model. *J Med Chem* DOI:10.1021/acs.jmedchem.5b01146 [published ahead of print].
Kempf DJ, Marsh KC, Denissen JF, McDonald E, Vasavanonda S, Flentge CA, Green BE, Fino L, Park CH, and Kong XP et al. (1995) ABT-538 is a potent inhibitor of human immunodeficiency virus protease and has high oral bioavailability in humans. *Proc Natl Acad Sci USA* **92**:2484–2488.
Kempf DJ, Marsh KC, Kumar G, Rodrigues AD, Denissen JF, McDonald E, Kukulka MJ, Hsu A, Granneman GR, and Baroldi PA et al. (1997) Pharmacokinetic enhancement of inhibitors of the human immunodeficiency virus protease by coadministration with ritonavir. *Antimicrob Agents Chemother* **41**:654–660.
Kena Diba A, Noll C, Richter M, Gieseler MT, and Kalesse M (2010) Intramolecular stereoselective protonation of aldehyde-derived enolates. *Angew Chem Int Ed Engl* **49**:8367–8369.
Kern D, Kern G, Neef H, Tittmann K, Killenberg-Jabs M, Wikner C, Schneider G, and Hübner G (1997) How thiamine diphosphate is activated in enzymes. *Science* **275**:67–70.
Klibanov OM, Gale SE, and Santevecchi B (2015) Ombitasvir/paritaprevir/ritonavir and dasabuvir tablets for hepatitis C virus genotype 1 infection. *Ann Pharmacother* **49**:566–581.
Koudriakova T, Iatsimirskaia E, Utkin I, Gangl E, Vouros P, Storozhuk E, Orza D, Marinina J, and Gerber N (1998) Metabolism of the human immunodeficiency virus protease inhibitors indinavir and ritonavir by human intestinal microsomes and expressed cytochrome P4503A4/3A5: mechanism-based inactivation of cytochrome P4503A by ritonavir. *Drug Metab Dispos* **26**:552–561.
Lin HL, Kent UM, and Hollenberg PF (2002) Mechanism-based inactivation of cytochrome P450 3A4 by 17 alpha-ethynylestradiol: evidence for heme destruction and covalent binding to protein. *J Pharmacol Exp Ther* **301**:160–167.
Mak PJ, Podstawka E, Kincaid JR, and Proniewicz LM (2004) Effects of systematic peripheral group deuteration on the low-frequency resonance Raman spectra of myoglobin derivatives. *Biopolymers* **75**:217–228.
Mak PJ, Zhu Q, and Kincaid JR (2013) Using resonance Raman cross-section data to estimate the spin state populations of cytochromes P450. *J Raman Spectrosc* **44**: 1792–1794.
Mansuy D, Battioni JP, Chottard JC, and Ullrich V (1979) Preparation of a porphyrin-iron-carbene model for the cytochrome P 450 complexes obtained upon metabolic oxidation of the insecticide synergists of the 1,3-benzodioxole series. *J Am Chem Soc* **101**:3971–3973.
Neese F (2012) The ORCA program system. *WIRES: Comp Mol Sci* **2**:73–78.
Neese F, Wennmohs F, Hansen A, and Becker U (2009) Efficient, approximate and parallel Hartree–Fock and hybrid DFT calculations. A 'chain-of-spheres' algorithm for the Hartree–Fock exchange. *Chem Phys* **356**:98–109.
Ortiz de Montellano PR (2005) *Cytochrome P450: structure, mechanism, and biochemistry*, 3rd ed, Kluwer Academic/Plenum, New York.
Podstawka E, Mak PJ, Kincaid JR, and Proniewicz LM (2006) Low frequency resonance Raman spectra of isolated alpha and beta subunits of hemoglobin and their deuterated analogues. *Biopolymers* **83**:455–466.
Rendic S (2002) Summary of information on human CYP enzymes: human P450 metabolism data. *Drug Metab Rev* **34**:83–448.
Ring BJ, Patterson BE, Mitchell MI, Vandenbranden M, Gillespie J, Bedding AW, Jewell H, Payne CD, Forgue ST, and Eckstein J et al. (2005) Effect of tadalafil on cytochrome P450 3A4-mediated clearance: studies in vitro and in vivo. *Clin Pharmacol Ther* **77**:63–75.
Ruf HH, Ahr H, Nastainczyk W, Ullrich V, Mansuy D, Battioni JP, Montiel-Montoya R, and Trautwein A (1984) Formation of a ferric carbanion complex from halothane and cytochrome P-450: electron spin resonance, electronic spectra, and model complexes. *Biochemistry* **23**:5300–5306.
Sevrioukova IF and Poulos TL (2010) Structure and mechanism of the complex between cytochrome P4503A4 and ritonavir. *Proc Natl Acad Sci USA* **107**: 18422–18427.
Sevrioukova IF and Poulos TL (2012) Interaction of human cytochrome P4503A4 with ritonavir analogs. *Arch Biochem Biophys* **520**:108–116.
Sevrioukova IF and Poulos TL (2013) Dissecting cytochrome P450 3A4-ligand interactions using ritonavir analogues. *Biochemistry* **52**:4474–4481.
Shaik S, Cohen S, Wang Y, Chen H, Kumar D, and Thiel W (2010) P450 enzymes: their structure, reactivity, and selectivity-modeled by QM/MM calculations. *Chem Rev* **110**:949–1017.
Shaik S, Kumar D, de Visser SP, Altun A, and Thiel W (2005) Theoretical perspective on the structure and mechanism of cytochrome P450 enzymes. *Chem Rev* **105**: 2279–2328.
Sugimoto H, Shinkyo R, Hayashi K, Yoneda S, Yamada M, Kamakura M, Ikushiro S, Shiro Y, and Sakaki T (2008) Crystal structure of CYP105A1 (P450SU-1) in complex with 1alpha,25-dihydroxyvitamin D3. *Biochemistry* **47**: 4017–4027.
Swart M, Güell M, Luis JM, and Solà M (2010) Spin-state-corrected Gaussian-type orbital basis sets. *J Phys Chem A* **114**:7191–7197.
Tao J, Perdew JP, Staroverov VN, and Scuseria GE (2003) Climbing the density functional ladder: nonempirical meta-generalized gradient approximation designed for molecules and solids. *Phys Rev Lett* **91**:146401.
Verras A, Alian A, and de Montellano PR (2006) Cytochrome P450 active site plasticity: attenuation of imidazole binding in cytochrome P450(cam) by an L244A mutation. *Protein Eng Des Sel* **19**:491–496.
von Moltke LL, Greenblatt DJ, Grassi JM, Granda BW, Duan SX, Fogelman SM, Daily JP, Harmatz JS, and Shader RI (1998) Protease inhibitors as inhibitors of human cytochromes P450: high risk associated with ritonavir. *J Clin Pharmacol* **38**:106–111.
Weigend F and Ahlrichs R (2005) Balanced basis sets of split valence, triple zeta valence and quadruple zeta valence quality for H to Rn: design and assessment of accuracy. *Phys Chem Chem Phys* **7**:3297–3305.
Wolf CR, Mansuy D, Nastainczyk W, Deutschmann G, and Ullrich V (1977) The reduction of polyhalogenated methanes by liver microsomal cytochrome P450. *Mol Pharmacol* **13**:698–705.
Zhao Y and Truhlar DG (2008) Density functionals with broad applicability in chemistry. *Acc Chem Res* **41**:157–167.

Address correspondence to: John C Hackett, Department of Physiology and Biophysics and the Massey Cancer Center, Virginia Commonwealth University School of Medicine, 401 College St. Richmond, Virginia, 23219. E-mail: john.hackett@vcuhealth.org